This article has been accepted for publication in a future issue of this journal, but has not been fully edited. Content may change prior to final publication. Citation information: DOI10.1109/TAP.2023.3247943, IEEE Transactions on Antennas and Propagation

Wideband Circularly Polarized Reflectarray Antenna Using Rotational Symmetrical Crossed Dipoles

Lehu Wen, Steven Gao, Qi Luo, Wei Hu, Benito Sanz-Izquierdo, and Xue-xia Yang

***Abstract*—A wideband circularly polarized (CP) reflectarray (RA) antenna using rotational symmetrical crossed dipoles is presented. This is the first time investigating coupled crossed dipoles as the unit cell for wideband reflection bandwidth in the CP RA design. Equivalent circuit analysis shows that when a CP wave impinges on the designed unit cell, two series resonances and two parallel resonances are simultaneously excited on the crossed dipoles. Owing to these four different resonances, the CP reflection bandwidth is greatly improved and elaborately adjusted by controlling the coupling between the crossed dipoles. The CP reflection bandwidth ratio of the unit cell is enhanced up to 2:1 for S_x<-15 dB with a thin thickness of $0.12\lambda_0$. Based on this unit cell, a wideband -20° collimated CP RA antenna with a circular aperture of 316 unit cells was designed, fabricated, and measured for final performance verification. The measured results show that a wide CP bandwidth of 7.6-15.9 GHz is achieved with the axial ratio <3 dB. In addition, the measured 3dB gain bandwidth is better than 43.7% with the peak realized gain of 26.3 dBic and the maximum aperture efficiency of 58.3%.**

***Index Terms*—Circular polarization, crossed dipoles, reflectarray antenna, wideband array antenna.**

I. Introduction

Owing to a planar reflector structure, reflectarray (RA) antennas have the advantages of simple configuration, easy fabrication, low product cost, and flexible desirable collimated beams compared to the traditional curved reflector antennas [1]. Therefore, they are widely applied in wireless communication systems, such as radars, satellites, etc. Because of the innate orientation immunity between the transmitting antenna and the receiving antenna, circular polarized (CP) antennas can have an additional channel-capacity improvement benefiting from the reduced multi-fading effect of the radiated CP wave [2]. As a result, a great number of CP RA antennas have been researched for wireless communications.

Depending on the feed type, there are normally two methods to realize CP RA antennas. The first method is utilizing a linearly polarized (LP) antenna as the feed to illuminate the reflector surface [3]-[6]. In this case, the RA elements are designed sensitively to the impinged orthogonal LP waves with an innate quadrature phase delay, and work as an LP to CP polarizer. However, CP RA antennas using this kind of feed method usually have a narrow operation bandwidth due to the limited phase bandwidth for LP-CP conversion. The second commonly used method is using a CP antenna as the feed. Its phasing methods can be versatile, such as using the length-variable phase delay line [7]-[8], the size-variable element [9]-[10], and the element rotation [11] for different wideband reflection phases. Among them, the element rotation method is widely applied in the RA design owing to its symmetrical and simple periodical phasing elements and a linear reflection phase response within the operation bandwidth. Utilizing this method, single I-shaped [12] and H-shaped [13] patches are used for wide CP reflection bandwidth with a single-layer structure. To further improve the CP reflection bandwidth, other different combinations of single-layered or multi-layered structures are utilized in the unit cell design [14]-[23]. In these RA designs, although wide axial ratio (AR) and gain bandwidths can be achieved by using the element rotation method, it is still a challenge to develop RA antennas with a wide operation bandwidth under a low-profile configuration.

In this work, unlike the traditional unit cells [12]-[21] using the H-shaped, I-shaped unit cells, or the combination of similar structures for wide CP reflection bandwidth, rotational symmetrical crossed dipoles are first investigated as the unit cell for designing a wideband CP RA antenna. This unit cell is composed of two-layered close-coupled arc-shaped crossed dipoles. Based on the circuit analysis, the coupling between the crossed dipoles can be elaborately utilized to introduce two different types of series and parallel resonances. Therefore, the CP reflection bandwidth of the designed unit cell can be greatly expanded with the resulted S_x<-15 dB bandwidth ratio up to 2:1 with a thin thickness of $0.12\lambda_0$. A high gain CP RA antenna with a tilted beam of -20° was then designed, fabricated, and measured using 316 unit cells. A wide 3dB AR bandwidth is measured covering 7.6-15.9 GHz (70.6%). The measured 3dB gain bandwidth is 10.2-15.9 GHz (43.7%) with the peak realized gain of 26.3 dBic and the max aperture efficiency (AE) of 58.3%. These good results prove that the designed unit cell can be widely applied in wideband high-gain wireless communication systems.

II. Unit Cell Design

A. Unit Cell Configuration

The configuration of the proposed RA unit cell for wideband CP radiation is shown in Fig. 1. As shown in the figure, the unit cell keeps a simple and rotational symmetrical structure. It is composed of two crossed arc-shaped dipoles, one dipole is x-axis arranged, and the other is y-axis arranged. At the end of the dipole arm, there is an arc-shaped strip with the radius of R2, arc of θ, and width of W3. The x-axis arranged dipole connects to the y-axis arranged dipole through a long and narrow arc-shaped strip with the radius of R1, arc of 270°, and width of W2. A shorting via with a diameter of 0.4 mm is located at the center of the unit cell to connect the different arms of the crossed dipoles. The conductors of the unit cell are printed on the top and bottom layers of a Rogers 4003C substrate with the relative permittivity of 3.55 and thickness of 0.508mm.

In the figure, the copper on the top layer of the unit cell is shown in orange color, and the copper on the bottom layer is shown in navy color. Under the Rogers substrate, a Rohacell foam [26] with the thickness of 3 mm and the relative permittivity of 1.04 is inserted to

This work was supported by Engineering and Physical Sciences Research Council under Grant EP/N032497/1, Grant EP/P015840/1, and Grant EP/S005625/1. *(Corresponding author: Lehu Wen.)*

L. Wen, S. Gao, and B. Sanz-Izquierdo are with the School of Engineering and Digital Arts, University of Kent, Canterbury, CT2 7NT, U.K. (e-mail: L.Wen@kent.ac.uk)

Q. Luo is with the School of Physics, Engineering and Computer Science, University of Hertfordshire, Hatfield, AL10 9AB, UK.

W. Hu is with the National Key Laboratory of Antennas and Microwave Technology, Xidian University, Xian, 710071, China.

X.-X. Yang is with the School of Communication and Information Engineering, Shanghai University, 200444, China.

This article has been accepted for publication in a future issue of this journal, but has not been fully edited. Content may change prior to final publication. Citation information: DOI10.1109/TAP.2023.3247943, IEEE Transactions on Antennas and Propagation

isolate the bottom copper layer from the ground plane. The performance of the unit cell is evaluated by EM software Ansys HFSS under the periodic boundary of the coupled lattice pair. The periodic size of the unit cell is 10 mm×10 mm, and its length is 0.52λ in free space at the highest working frequency.

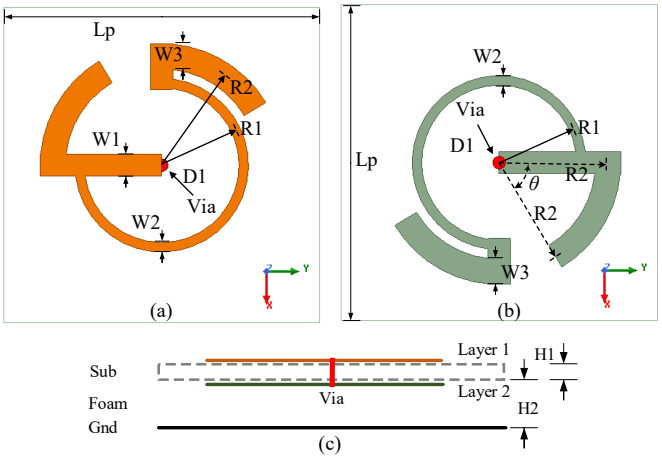

Fig. 1. Configuration of the wideband unit cell for CP radiation. (a) Top Layer. (b) Lower layer. (c) Side view. (Detailed parameters in the design, Lp=10 mm, D1=0.4 mm, W1=0.7 mm, W2=0.3 mm, W3=0.8 mm, R1=2.6 mm, R2=3.5 mm, θ=59°, H1=0.508 mm, H2=3 mm.)

B. Reflection Bandwidth

In the performance evaluation of the unit cell, TE and TM polarized waves impinging on the surface of the unit cell are utilized to obtain the corresponding reflection coefficients for the co-polarized and cross-polarized CP waves. In this work, the RA antenna is designed for RHCP radiation, so its co-polarized and cross-polarized S-parameters can be calculated as [24],

$$S_{co} = \left[\frac{S_{11} - S_{22}}{2} + jS_{12}\right] e^{j2\alpha} \quad (1)$$

$$S_x = \frac{S_{11} + S_{22}}{2} \quad (2)$$

where α is the element rotation angle, the subscripts 1 and 2 in S-parameters represent the impinged TE mode and TM mode waves respectively. Note that (1) also indicates that a α rotation angle will cause a 2α phase shift for the reflected wave.

Based on (1)-(2), the EM simulated S-parameters of the proposed unit cell for RHCP radiation are evaluated and shown in Fig. 2. A strong and wideband reflection is achieved for the normal-impinged co-polarized CP wave. Compared to other unit cell designs in Table I, a low cross-polarization level with a wider bandwidth of 7.7-15.5 GHz (ratio=2:1, FBW=67.2%) for S_x<-15 dB is achieved. Note that the cross-polarization level of S_x<-15 dB is equivalent to AR<3 dB for the reflected CP wave. In addition, four cross-polarized reflection zeros are observed, and these four reflection zeros are located at 8 GHz, 9.6 GHz, 12.8 GHz, and 14.8 GHz. Owing to the four reflection zeros, the bandwidth can be significantly increased compared to other traditional unit cells. Note that the EM software Ansys HFSS is used to design both the unit cell and CP RA antenna.

The strong and wideband reflection for the impinged CP wave originates from the four resonances in the unit cell. Fig. 3 gives a simplified equivalent circuit of this unit cell. As shown in the figure, when the electric field of the impinged CP wave is in y-axis direction, the arc-shaped dipole arm can be equivalent to a series resonant circuit, which is composed of an inductor L_1 and a capacitor C_1 shorted to the ground. The capacitance C_1 is mainly from two different interactions, which are the capacitance between the arc end and the ground plane and the minor effect of the coupling between the adjacent dipole arms. In addition, the center y-axis arranged line-strip can be equivalent to a parallel resonant circuit, which is composed of an inductor L_2 and a capacitor C_2. Therefore, considering the overall effects, a combination of the series resonance and the parallel resonance can be simultaneously excited when the E-field of the impinged CP wave is in y-axis direction.

Similarly, after a quarter of the oscillation period, when the electric field of the impinged CP wave is in x-axis direction, the arc-shaped dipole arm can be equivalent to a series resonant circuit, which is composed of an inductor L_3 and a capacitor C_3 shorted to the ground. Additionally, the narrow strip with the arc angle of 270° can be equivalent to a parallel resonant circuit, which is composed of an inductor L_4 and a capacitor C_4. Therefore, another combination of the series resonance and the shunt resonance can be achieved when the E-field of the impinged CP wave is in x-axis direction. Overall, there are four different resonances in series and parallel, as the E-filed varies consecutively in two orthogonal directions.

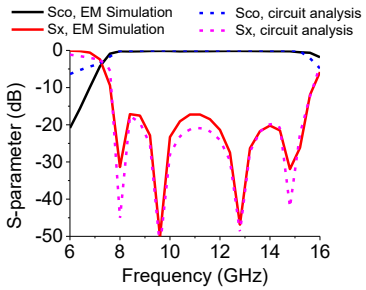

Fig. 2. Simulated co-polarized and cross-polarized S-parameters of the proposed unit cell under normal incidence.

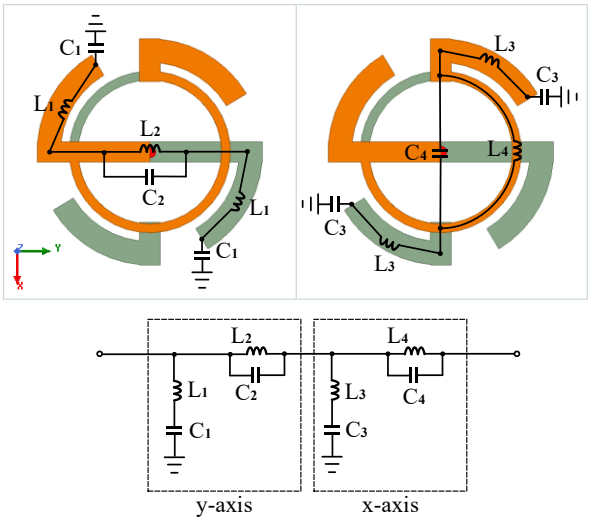

Fig. 3. Simplified equivalent circuit of the proposed unit cell. (Lumped component values, L1=1.57 nH, C1=0.25 pF, L2=0.45 nH, C2=0.35 pF, L3=0.9 nH, C4=0.3 pF, L4=0.24 nH, C4=0.48 pF.)

The S-parameter response calculated from the equivalent circuit is added in Fig. 2 for a good comparison to the EM simulated results. The values of the lumped components are also calculated [27] and shown in the caption of Fig. 3. It can be seen that, although a simplified circuit is used for equivalence, four cross-polarized zeroes are well predicted by the equivalent circuit with good in-band accordance. Due to the other minor distributed parasitic parameters and Q-effect in the unit cell, some small discrepancies can also be found in and out of the bandwidth. However, this has no effect in illustrating the basic working principle of the proposed unit cell.

This article has been accepted for publication in a future issue of this journal, but has not been fully edited. Content may change prior to final publication. Citation information: DOI10.1109/TAP.2023.3247943, IEEE Transactions on Antennas and Propagation

The simulated S-parameters of the proposed unit cell under the normal-impinged orthogonal TE and TM waves are shown in Fig. 4. For the magnitude response shown in Fig. 4 (a), it can be seen that, the impinged TE and TM waves do not have a perfect reflection as the traditional symmetrical unit cell for CP RA design, and the reflection coefficients are almost flat and linear, and close to -6 dB within the bandwidth. The impinged TE mode wave can partially reflect into TM mode wave, and the transmission coefficient is also very flat, and close to -1.4 dB within the bandwidth. Unlike the traditional unit cell discussed in [24], these two orthogonal modes do not have a perfect isolation. However, it does not affect the presented unit cell to be a good element for wideband CP reflection bandwidth.

Fig. 4 (b) gives the phase responses of the unit cell under different normal-impinged modes. It can be seen that the phase difference curve has one peak and two valleys, which introduces four cross-points with the horizontal line of 180° phase difference. The corresponding frequencies of these four cross-points have a good consistency with the four cross-polarized reflection zeros shown in Fig. 2. From this figure, it can be found that, as indicated in (2), as long as the reflection coefficients of these two orthogonal modes have the same magnitude but out-of-phase difference, high co-polarized reflection can be achieved for CP radiation.

C. *Performance Investigation*

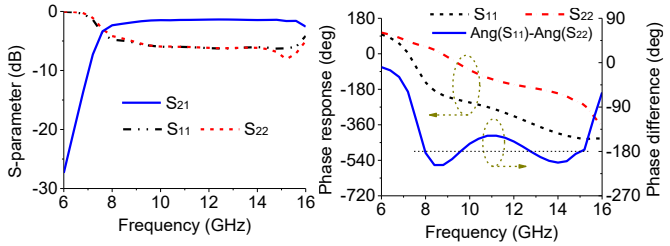

(a) (b)

Fig. 4. HFSS-simulated S-parameter responses of (a) magnitude and (b) phase of the proposed unit cell under the normal-impinged TE and TM waves.

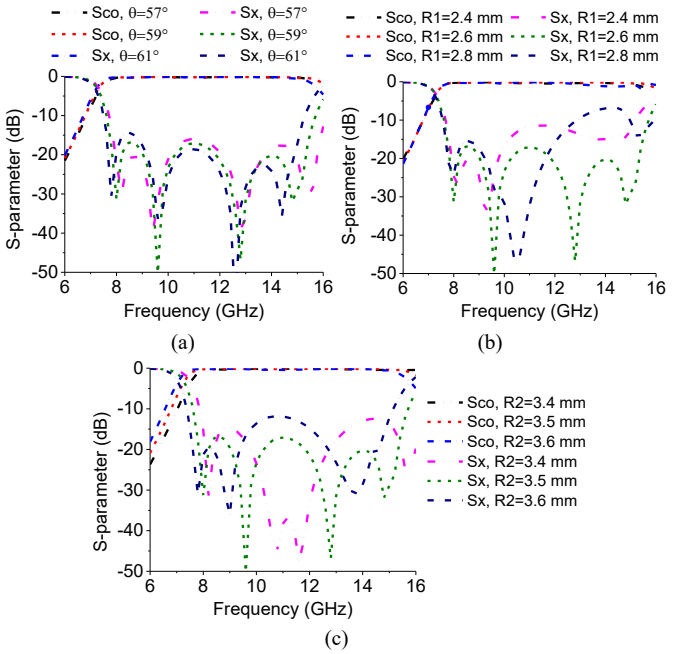

(a) (b) (c)

Fig. 5. HFSS-simulated effects of the (a) dipole arm arc θ, (b) dipole arm radius R2, and (c) narrow arc radius R1 on the performance of the unit cell.

In the design of the proposed unit cell, it is found that the dipole arm arc θ, dipole arm radius R2, and narrow arc radius R1 can have significant effects on the performance of the co-polarized and cross-polarized S-parameters for CP radiation. Fig. 5 shows the simulated different effects of these parameters. First, in Fig. 5 (a), when the dipole arm arc θ is increased from 57° to 61°, it is observed that only the first and the fourth cross-polarized reflection zeros are moved clearly, while the other two reflection zeros are slightly shifted. This is because when only the arc θ varies, the center structure parameters are unaffected, so the parallel resonances will not be affected.

Fig. 5 (b) shows the effect of the dipole arm radius R2 on the performance of the unit cell. It can be seen that as the increase of R2, all the resonant frequencies of the cross-polarized S-parameters are changed clearly. This is because when R2 increases, the center structure will be extended accordingly, so the parallel resonances will also be changed. In addition, as R2 increases, the dipole arm arc-length is increased, which denotes the series resonances are also changed. Therefore, the overall operation bandwidth will move to the lower frequency when R2 is increased, as indicated in the figure.

The effect of the narrow arc radius R1 on the performance of the unit cell is shown in Fig. 5 (c). It can be seen that, when R1 is increased from 2.4 mm to 2.8 mm, only the third cross-polarized zero is clearly changed, while the other resonant frequencies are slightly moved. According to the equivalent circuit, the change of the narrow arch radius R1 will have a great effect on the parallel resonance in the x-axis direction. Therefore, this reflection zero changes clearly as the variance of the narrow arc radius.

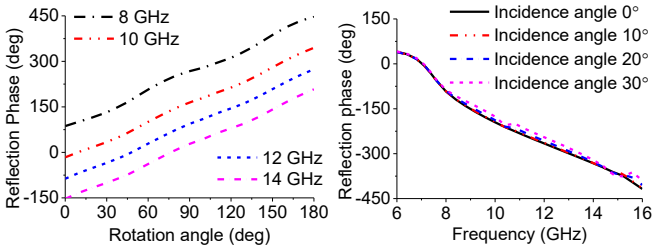

(a) (b)

Fig. 6. HFSS-simulated reflection phase of the proposed unit cell with (a) different rotation angles and (b) different incident angles.

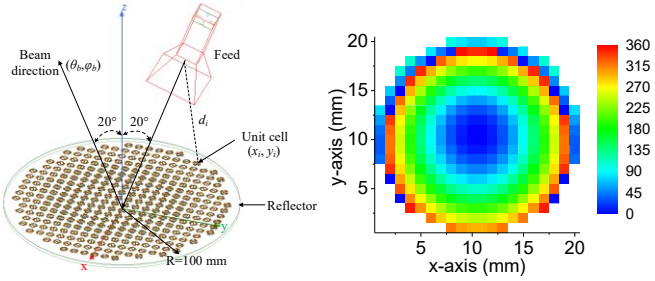

(a) (b)

Fig. 7. (a) Configuration of the proposed CP RA antenna and (b) phase distribution of the unit cells.

In the CP RA antenna design, the element rotation technique [11] is used to obtain a proper CP reflection phase for each unit cell. To evaluate the reflection phase performance, the co-polarized reflection phase changing with different rotation angles is studied and shown in Fig. 6 (a). It can be seen that the reflection phase varies linearly with the element rotation angle, so an accurate reflection phase can be achieved by rotating the unit cell. Fig. 6 (b) gives the reflection phase of the unit cell under different incident angles. It can be seen that, when the incident angle increases, minor discrepancies can be observed in the reflection phase. At the oblique incident angle of 30°, a small phase error of maximum 25.7° can be observed. Therefore, with the results shown in Fig. 6 (a) and Fig. 6 (b), a wideband CP RA antenna can be expected by using the proposed unit cell.

This article has been accepted for publication in a future issue of this journal, but has not been fully edited. Content may change prior to final publication. Citation information: DOI10.1109/TAP.2023.3247943, IEEE Transactions on Antennas and Propagation

III. Reflectarray Design

A. Array Configuration

The configuration of the CP RA antenna is shown in Fig. 7 (a). It is composed of the designed RA reflector and an offset feed. The RA reflector is in a circular shape with an aperture radius of 100 mm of 316 elements. A feed horn antenna is designed with an operation bandwidth covering 7.5-15.5 GHz for RHCP radiation, and its gain is around 14 dBic. The RA reflector is illuminated by this feed with an offset angle of 20° to avoid the feed blockage, which is placed in yz-plane. The beam direction is also in the same yz-plane, and symmetrical to the feed offset direction with an angle of -20° off the +z direction. The focal to diameter ratio (f/D) is designed as 0.9 to maintain a high AE balance for both high illumination and low spillover within the operation bandwidth.

Based on the RA configuration shown in Fig. 7 (a), the required phase distribution $\emptyset_R$ of each unit cell can be calculated using the below equation [1],

$$\emptyset_R = k_0(d_i - (x_i cos\varphi_b + y_i sin\varphi_b)sin\theta_b) \quad (3)$$

where k_0 is the propagation constant in vacuum, d_i is the distance of the phase center of the feed to the unit cell i, (x_i, y_i) is the coordinate of unit cell i, and (θ_b, φ_b) is the array beam direction. Therefore, the calculated phase distribution at the center frequency of 11 GHz is obtained and shown in Fig. 7 (b). The detailed rotation angle of each unit cell can be obtained according to the required reflection phase.

B. Feed and Aperture Size Consideration

To accommodate the wide operation bandwidth of the proposed unit cell, the RA feed should be carefully designed with enough wide bandwidth to illuminate the designed RA reflector. Therefore, a wideband four-feed CP horn antenna [23] is designed as the feed for the proposed CP RA reflector, and the designed horn antenna is shown in Fig. 7 (a). In addition, a broadband 1 to 4 power divider with a sequential quadrature phase delay [25] is designed and incorporated to excite the horn antenna for wideband CP radiation.

When designing the selected RA feed, an ideal square waveguide is introduced and compared in the CP RA design. The performances of the proposed RA reflector illuminated by the practical horn antenna are very close to that is illuminated by an ideal waveguide. The figure inset into the top of Fig. 8 shows the configurations of the ideal square waveguide and the practically used four-feed horn in this design. Note that the ideal square waveguide is excited by a wave port with two orthogonal modes and a 90° phase delay for wideband CP radiation. While the horn antenna is excited by four lumped ports with equal magnitude and sequential 90° phase delay for CP radiation. To keep the same radiation characteristics in terms of beamwidth and directivity, these two feeds are designed with the same square radiation aperture of 50×50 mm^2.

As shown in Fig. 8 (a), both AR and AE bandwidths of the proposed RA reflector illuminated by these two different feeds are almost the same. A slight frequency shift to the lower frequency can be seen due to the difference in their impedance bandwidth. It can also be observed that the simulated peak AE illuminated by the practical horn antenna is slightly lower than the ideal square waveguide. The peak AE is 61.9% at 11 GHz for the ideal square waveguide, while the simulated peak AE is 59.3% at 11.2 GHz for the four-feed horn. The decrease in AE is mainly from the reduced efficiency and instable phase center for the practical horn antenna compared to the ideal square waveguide.

Fig. 8 (b) compares the peak realized gain of the RA antenna illuminated by these two different feeds. Owing to the elaborately designed feed, the simulated gains have a good accordance with each other. The gain illuminated by the four-feed horn is only slightly reduced within the bandwidth, compared to the ideal square waveguide. The peak realized gains of the two feeds are also shown for comparison. It can be seen that the ideal square waveguide has a very ideal gain, which is almost as linear as the frequency. However, the gain of the practical horn antenna can only keep linear from 7.5 GHz to 15.5 GHz. Once the frequency is away from the bandwidth, the gain is decreased sharply. In addition, due to the increased loss in the transition junction of the horn, the realized gain of the horn antenna is slightly reduced compared to the ideal square waveguide.

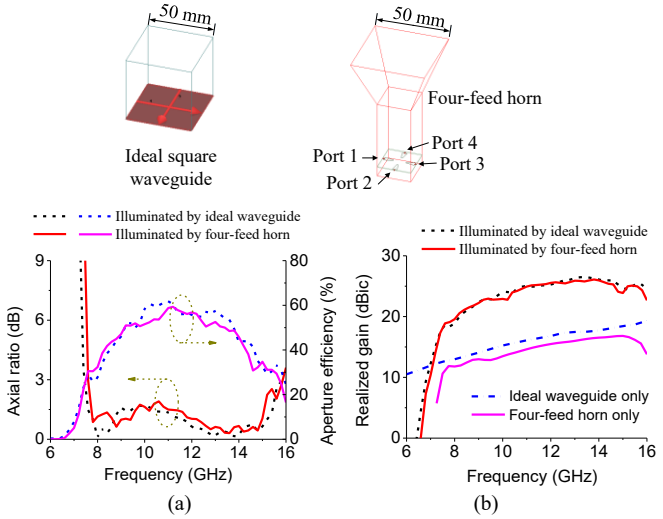

Fig. 8. Performances of (a) AR and AE and (b) peak realized gain of the presented RA antenna when illuminated by different feed antennas.

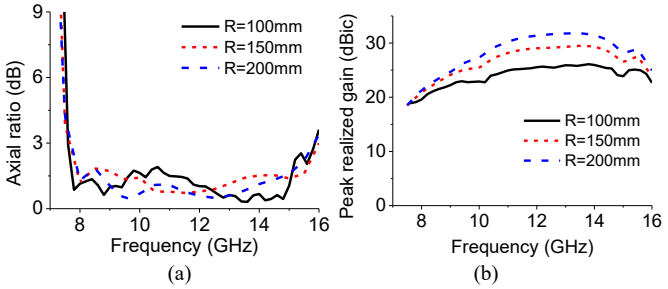

Fig. 9. Performances of (a) AR and (b) peak realized gain of the designed RA antenna with different aperture sizes.

With the comparison between the ideal feed and the practical horn antenna, it can be seen that a good accordance is achieved for the developed RA reflector, when it is illuminated by both the ideal and the practical feeds. This can promise that the presented RA antenna can have a wide AR bandwidth covering 7.4-15.2 GHz and a maximum peak AE of around 59.3% when illuminated by the designed four-feed horn antenna.

Fig. 9 shows the radiation performances of the designed CP RA antenna with different aperture sizes. In the radiation performance investigation, two larger apertures with the radius R=150mm (716 elements) and the radius R=200 mm (1264 elements) are designed and simulated for performance comparison. All the large-scale CP RA antennas have the same F/D ratio and use the same feed. It can be seen in Fig. 9 (a) that the AR bandwidths of these three different aperture radii are almost the same, and the simulated AR values are lower than 2 dB within the entire bandwidth. This good accordance confirms the excellent wideband CP radiation characteristic of the proposed unit cell. Fig. 9 (b) shows the gains of these three different

This article has been accepted for publication in a future issue of this journal, but has not been fully edited. Content may change prior to final publication. Citation information: DOI10.1109/TAP.2023.3247943, IEEE Transactions on Antennas and Propagation

RA apertures. It can be seen that, the gain curves in the lower-half frequency band keep nearly linear as the increase of frequency, and gradually become horizontal due to the reduced illumination efficiency in the upper-half frequency band. Overall, these results show the robustness of the proposed unit cell against the differential spatial phase delay. Owing to the proposed wideband unit cells, the developed CP RA antennas can have stable and consistent radiation performances when the aperture size increases.

C. Results

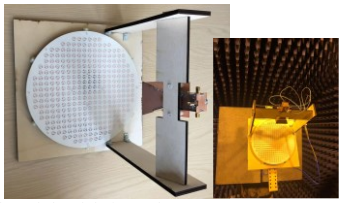

Fig. 10. Photographs of the fabricated CP RA antenna.

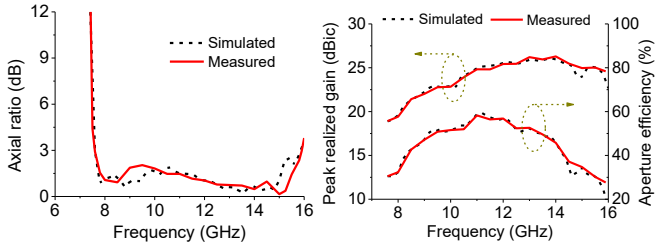

Fig. 11. (a) Measured and simulated AR and (b) peak realized gains and aperture efficiencies of the presented CP RA antenna.

The proposed wideband CP RA antenna was designed, fabricated, and measured at the University of Kent for the final performance verification. Fig. 10 shows the photographs of the fabricated CP RA prototype and the prototype measured in the anechoic chamber for radiation performance. The measured AR is shown in Fig. 11 (a), which is also compared with the simulated AR. As shown in the figure, the measured CP bandwidth for AR<3dB is 7.6-15.9 GHz, which is slightly wider than the simulated AR bandwidth, and has a slight shift to the upper frequency. The measured AR curve has a good tendency with the simulated curve.

The measured peak realized gain and AE are shown in Fig. 11 (b). Compared to the simulated curves, the measured results agree well with them. The measured peak realized gain varies from 18.9 dBic to 24.6 dBic with the maximum gain of 26.3 dBic at 14 GHz within the AR bandwidth. The measured 3 dB gain bandwidth is 10.2-15.9 GHz. The measured 30% AE bandwidth is 7.6-15.5 GHz, and 50% AE bandwidth is 9.2-13.5 GHz with the maximum AE value of 58.3%, which is slightly lower than the simulated peak AE.

The measured normalized radiation patterns of the proposed CP antenna at the frequencies of 8 GHz, 10 GHz, 12 GHz, and 14 GHz are shown in Fig. 12. It should be noted that in the figure, the co-polarized radiation patterns are the RHCP patterns, and the cross-polarized radiation patterns are the LHCP patterns. First, as can be seen in yz-plane, both the measured radiation patterns have a good accordance with the simulated radiation patterns. The radiated beams can point exactly to -20° as the designed beams. The sidelobe levels keep around 20 dB lower than the main beam at both beam sides. The measured half-power beamwidth in this plane varies from 17° to 7° as the increase of working frequency.

The measured normalized radiation patterns in xz-plane (in the beam direction) are also incorporated and shown in this figure. Similarly, a very good accordance is achieved between the simulated radiation patterns and the measured radiation patterns, especially in the main beam direction. The sidelobe levels also keep around 20 dB lower than the main beam at both two beam sides. The measured half-power beamwidth in this plane varies from 12° to 8° as the working frequency increases. The discrepancies between the simulated and measured results are mainly due to the manufacture errors and assembly errors in the antenna fabrication. In addition, the position errors in the anechoic chamber can have a slight effect on the accuracy of the measured radiation performances.

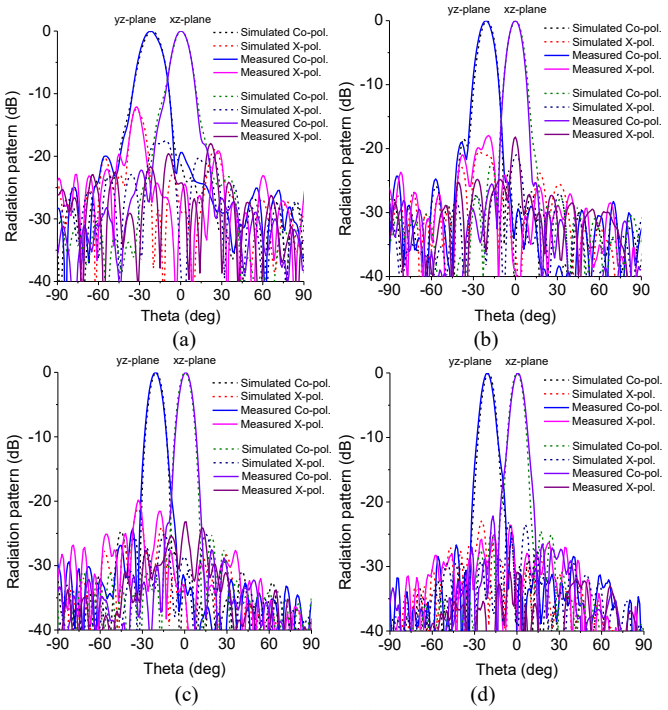

Fig. 12. Normalized radiation patterns of the proposed CP RA antenna in yz-plane and xz-plane (in the beam direction) at (a) 8 GHz, (b) 10 GHz, (c) 12 GHz, and (d) 14 GHz.

D. Comparison

Table I compares the presented array antenna with the recently published CP RA antennas. In this table, λ_0 is the free space wavelength at the center operation frequency. CP RA antennas in [3]-[5] use the LP antenna as the feed for the reflector. Due to the limitation of the conversion bandwidth from the LP wave to the CP wave, the obtained AR bandwidths of these RA antennas are normally limited and not wide enough for the wide bandwidth required wireless communications. [7]-[10] are the methods of using the length-variable phase delay line or size-variable element for CP RA design. In these traditional methods, the CP reflection bandwidth is normally not considered in the unit cell design, and only the reflection phase varying with the length or size is studied for CP RA design. Therefore, the related AR bandwidths are not wide enough (around 15%), and normally narrower than the gain bandwidth.

The RA antennas in [18], [22], and [23] use the wideband CP horn antenna as the feed, in which the element rotation method is utilized for the wideband CP reflection phase, and a wide AR bandwidth of more than 40% can be achieved in these works. Compared to these CP RA antennas, owing to the elaborately introduced four cross-polarized reflection zeros, a wide CP reflection bandwidth of 67.2% for S_x<-15 dB is realized for the presented unit cell. Accordingly, a wide AR bandwidth of 70.6% is obtained for the designed RA antenna. It should be noted that although the obtained 3dB gain

This article has been accepted for publication in a future issue of this journal, but has not been fully edited. Content may change prior to final publication. Citation information: DOI10.1109/TAP.2023.3247943, IEEE Transactions on Antennas and Propagation

bandwidth is slightly narrower than the gain bandwidth in [23], the developed CP RA antenna has a smaller thickness and a more stable variance in both gain and AE compared to this reference RA antenna, which is benefiting from the wide reflection bandwidth of the presented unit cell. In addition, our proposed antenna has a high peak gain of 26.3 dBic and a relatively low profile with the F/D of 0.9 and the reflector thickness of $0.12\lambda_0$.

TABLE I
COMPARISON OF THE RECENTLY PUBLISHED CP RA ANTENNAS

Ref.	Unit cell BW	3dB AR BW	3dB gain BW	Aperture $\lambda_0\times\lambda_0$	Thick-ness (λ_0)	F/D	Peak gain (dBic)	Peak AE
[3]	29.7%	28%	33%	4.16×4.16	0.13	1	19.4	44%
[4]	/	12.5%	12.8%	5.56×5.56	0.11	1.2	20.4	30%
[5]	/	25.8%	50%	6.66×6.66	0.12	0.84	24.5	46.3%
[7]	/	14.6%	15.6%	7.97×7.97	0.03	1	25.3	45%
[8]	/	23.7%	25%	4.43×4.43	0.05	1	17.1	20%
[9]	/	10%	12.3%	π×14×14	0.05	0.618	36.7	60.4%
[10]	/	11%	15%	9×9	0.07	0.98	25.8	39%
[18]	44.2%	40%	28.5%	4.76×4.76	0.13	0.7	22.5	52.3%
[22]	38.5%	42%	41.8%	6.1×6.1	0.11	1.2	25.4	60%
[23]	62.9%	68.5%	47.8%	6.4×6.4	0.14	0.97	25.2	60%
This work	67.2%	70.6%	43.7%	π×3.9×3.9	0.12	0.9	26.3	58.3%

IV. CONCLUSION

A new unit cell using symmetrical rotational crossed dipoles for wideband CP RA antenna design has been proposed. The unit cell keeps a low profile while having a wide CP reflection bandwidth ratio of 2:1. Equivalent circuit and parametrical studies are given to illustrate the working principle of the proposed unit cell. A wideband CP RA antenna with a tilted beam of -20° was developed and measured for performance verification. The measured 3dB AR bandwidth is 7.6-15.9 GHz (70.6%), and 3dB gain bandwidth is 10.2-15.9 GHz (43.7%). A high peak realized gain of 26.3 dBic is achieved with the maximum AE of 58.3%. Good agreement between the simulated and measured results demonstrates that the developed CP RA antenna can be a good candidate for wideband high-gain wireless communications.

REFERENCES

[1] J. Huang and J. A. Encinar, *Reflectarray Antennas*. New York, NY, USA: IEEE Press, 2008.

[2] L. Wen et al., "Compact and wideband crossed dipole antenna using coupling stub for circular polarization," *IEEE Trans. Antennas Propag.*, vol. 70, no. 1, pp. 27-34, Jan. 2022.

[3] L. Ren, Y. Jiao, F. Li, J. Zhao and G. Zhao, "A dual-layer T-shaped element for broadband circularly polarized reflectarray with linearly polarized feed," *IEEE Antennas Wireless Propag. Lett.*, vol. 10, pp. 407-410, 2011.

[4] S. R. Lee, E. H. Lim, F. L. Lo and W. H. Ng, "Circularly polarized elliptical microstrip patch reflectarray," *IEEE Trans. Antennas Propag.*, vol. 65, no. 8, pp. 4322-4327, Aug. 2017.

[5] G. Wu, S. Qu, S. Yang and C. H. Chan, "Broadband, single-layer dual circularly polarized reflectarrays with linearly polarized feed," *IEEE Trans. Antennas Propag.*, vol. 64, no. 10, pp. 4235-4241, Oct. 2016.

[6] G. -T. Chen, Y. -C. Jiao, G. Zhao and C. -W. Luo, "Design of wideband high-efficiency circularly polarized folded reflectarray antenna," *IEEE Trans. Antennas Propag.*, vol. 69, no. 10, pp. 6988-6993, Oct. 2021.

[7] R. S. Malfajani and Z. Atlasbaf, "Design and implementation of a broadband single layer circularly polarized reflectarray antenna," *IEEE Antennas Wireless Propag. Lett.*, vol. 11, pp. 973-976, 2012.

[8] S. Mener, R. Gillard, R. Sauleau, C. Cheymol and P. Potier, "Design and characterization of a CPSS-based unit-cell for circularly polarized reflectarray applications," *IEEE Trans. Antennas Propag.*, vol. 61, no. 4, pp. 2313-2318, April 2013.

[9] R. Deng, Y. Mao, S. Xu and F. Yang, "A single-layer dual-band circularly polarized reflectarray with high aperture efficiency," *IEEE Trans. Antennas Propag.*, vol. 63, no. 7, pp. 3317-3320, July 2015.

[10] G. Zhao, Y. Jiao, F. Zhang and F. Zhang, "A subwavelength element for broadband circularly polarized reflectarrays," *IEEE Antennas Wireless Propag. Lett.*, vol. 9, pp. 330-333, 2010.

[11] J. Huang, and R. J. Pogorzelski, "A ka-band microstrip reflectarray with elements having variable rotation angles," *IEEE Trans. Antennas Propag.,* vol. 46, no. 5, pp. 650-656, 1998.

[12] W. Guo, G. Wang, K. Liu, Y. Zhuang and Q. Ge, "Design of single-layered ultrawideband high-efficiency circularly polarized reflectarray," *IEEE Antennas Wireless Propag. Lett.*, vol. 17, no. 8, pp. 1386-1390, Aug. 2018.

[13] W.-L. Guo, G.-M. Wang, W.-Y. Ji, Y.-L. Zheng, K. Chen and Y. Feng, "Broadband spin-decoupled metasurface for dual-circularly polarized reflector antenna design," *IEEE Trans. Antennas Propag.*, vol. 68, no. 5, pp. 3534-3543, May 2020.

[14] M. Veljovic and A. K. Skrivervik, "Ultralow-profile circularly polarized reflectarray antenna for cubesat intersatellite links in K-band," *IEEE Trans. Antennas Propag.*, vol. 69, no. 8, pp. 4588-4597, Aug. 2021.

[15] M. -Y. Zhao, G. -Q. Zhang, X. Lei, J. -M. Wu and J. -Y. Shang, "Design of new single-layer multiple-resonance broadband circularly polarized reflectarrays," *IEEE Antennas Wireless Propag. Lett.*, vol. 12, pp. 356-359, 2013.

[16] T. Smith, U. Gothelf, O. S. Kim and O. Breinbjerg, "An FSS-backed 20/30 GHz circularly polarized reflectarray for a shared aperture L- and Ka-band satellite communication antenna," *IEEE Trans. Antennas Propag.*, vol. 62, no. 2, pp. 661-668, Feb. 2014.

[17] X. Yang et al., "A broadband high-efficiency reconfigurable reflectarray antenna using mechanically rotational elements," *IEEE Trans. Antennas Propag.*, vol. 65, no. 8, pp. 3959-3966, Aug. 2017.

[18] Q. Gao, J. Wang, Y. Li and Z. Li, "A multiresonant element for bandwidth enhancement of circularly polarized reflectarray antennas," *IEEE Antennas Wireless Propag. Lett.*, vol. 17, no. 5, pp. 727-730, May 2018.

[19] P. Naseri and S. V. Hum, "A dual-band dual-circularly polarized reflectarray for K/Ka-band space applications," *2019 13th European Conf. Antennas Propag. (EuCAP)*, 2019, pp. 1-5.

[20] B. Li, C. Y. Mei, Y. Zhou and X. Lv, "A 3-D-printed wideband circularly polarized dielectric reflectarray of cross-shaped element," *IEEE Antennas Wireless Propag. Lett.*, vol. 19, no. 10, pp. 1734-1738, Oct. 2020.

[21] A. Mahmoud, A. A. Kishk, Z. Hao and W. Hong, "Ka-band circularly polarized reflectarray: Using a double-layers cross slot," *IEEE Antennas Propag. Magazine*, vol. 58, no. 4, pp. 60-68, Aug. 2016.

[22] F. Wu, J. Wang, Y. Zhang, W. Hong and K. -M. Luk, "A broadband circularly polarized reflectarray with magneto-electric dipole elements," *IEEE Trans. Antennas Propag.*, vol. 69, no. 10, pp. 7005-7010, Oct. 2021.

[23] L. Zhang, S. Gao, Q. Luo, W. Li, Y. He and Q. Li, "Single-layer wideband circularly polarized high-efficiency reflectarray for satellite communications," *IEEE Trans. Antennas Propag.*, vol. 65, no. 9, pp. 4529-4538, Sept. 2017.

[24] A.Boriskin and R. Sauleau, *Aperture Antennas for Millimeter and Sub-Millimeter Wave Applications*. New York, NY, USA: Springer, 2017.

[25] W. Hu et al., "Wideband circularly polarized antenna using single-arm coupled asymmetric dipoles," *IEEE Trans. Antennas Propag.*, vol. 68, no. 7, pp. 5104-5113, July 2020.

[26] Rohacell HF product information, accessed: Oct. 2021. [Online]. Available: https://performance-foams.evonik.com/en/downloads.

[27] J.-S. Hong and M. J. Lancaster, *Microstrip Filters for RF/Microwave Applications*. New York, NY, USA: Wiley, 2001.